**Canadian Conference - Pacific Conference on Earthquake Engineering 2023**
**Vancouver, British Columbia**
**June 25th – June 30th, 2023**

# Influence Of Pile Group Effect Modeling Methods On Seismic Behavior Of Piles-supported Bridges

Lianxu Zhou[1*], Aijun Ye[2] and M. Shahria Alam[3]

[1]PhD, State Key Laboratory of Disaster Reduction in Civil Engineering, Tongji University, Shanghai, China; The postdoctoral research fellow of the University of British Columbia, Kelowna, BC V1V 1V7, Canada.
[2]Professor, State Key Laboratory of Disaster Reduction in Civil Engineering, Tongji University, Shanghai, China
[3]Professor, School of Engineering, University of British Columbia, Kelowna, BC, Canada
[*]lianxuzhou19@gmail.com (Corresponding Author)

## ABSTRACT

Pile group foundations are commonly utilized in bridge engineering. The earthquake-induced damage or nonlinear behavior of piles has been reported in previous earthquake events. Therefore, the accurate seismic demand prediction for pile group-supported bridges considering the soil pile interaction is crucial in the phase of seismic design and performance assessment for the pile-supported bridges. For the pile group foundations, the pile group effect modeling is a critical issue in finite element modeling. However, the existing pile group efficiency method cannot describe the lateral resistance difference among different pile rows when the pile group-supported bridge is subjected to earthquake loadings, resulting in an inaccurate estimation of the nonlinear behavior. To this end, this study introduces a practical pile-group effect modeling method for the pile group when they are subjected to earthquake loadings. Furthermore, the influence of different pile group effect modeling methods on the seismic behavior of pile-supported bridges is investigated in this study. The results show that the pile group effect modeling method proposed in this study can better predict the nonlinear seismic behavior of pile group-supported bridges. The commonly used pile group efficiency method could underestimate the seismic demand or fragility of the pile head. The pile group effect modeling methods slightly affect the global seismic response of the pile group supported bridges, including the pier curvature and bearing displacement demand.

Keywords: Soil pile interaction; Pile group effect; Seismic fragility; Bridge scour; pile group foundation.

## INTRODUCTION

Pile group foundations are commonly utilized in bridge engineering. Previous studies found that the scour makes the pile foundation more prone to earthquake-induced damage. Therefore, the nonlinear behavior of pile foundations under the combined effects of scour and earthquake is drawing increasing attention from the engineering and academic communities. Zhou et al.[1], Liu et al. [2] and Wang et al. [3] carried out a series of quasi-static tests to investigate the seismic failure mechanism of pile group foundations with socur effects. These experiments reported that the leading pile carried the most proportion of lateral loads. As a result, the leading pile is more prone to earthquake-induced damage. When a pile group is subjected to earthquake shakings, the pile in the loading directions could repeatedly change from a leading pile to a trailing pile. However, how to accurately model the pile group effect, especially for closely spaced piles, has not been addressed in previous studies, in which they usually adopted a constant reduction factor (i.e., pile group efficiency) to discount the ultimate capacity of the *p-y* spring for a single pile [4,5]. Such treatment cannot describe the lateral resistance difference among different pile rows when the pile group supported bridge is subjected to cyclic loads such as earthquake loadings, resulting in an inaccurate estimation of the pile curvature.

This study introduces a practical modeling method for pile group foundations under seismic loads. After that, we investigated the sensitivity of the soil element mesh on the seismic behavior of a soil-bridge system. Finally, the influence of pile group effect modeling methods on the seismic behavior of the soil pile-bridge system are discussed.

## PILE GROUP EFFECT MODELING METHODS

The pile group effect is a crucial issue in the finite element modeling for the pile group supported bridges considering soil pile interaction. The soil resistance of a single pile without pile group effect is described as follows [6,7]:

$$p = A \cdot p_u \cdot \tanh\left(\frac{n_h \cdot h}{A \cdot p_u} \cdot y\right) \tag{1}$$

$$p_u = \min(p_{us}, p_{ud}) \tag{2}$$

$$p_{us} = (C_1 \cdot h + C_2 \cdot D) \cdot \gamma \cdot h \tag{3}$$

$$p_{ud} = C_3 \cdot D \cdot \gamma \cdot h \tag{4}$$

where $p$ is the lateral resistance of soil at the embedded depth $h$. $y$ denotes the lateral deflection of the pile at depth $h$. $p_u$ is the ultimate resistance of the sand at depth $h$. $A$ is a loading factor, which is equal to 0.9 for cyclic loading; $p_{us}$ and $p_{ud}$ denote the ultimate resistance of soil in the shallow and deep regions, respectively. $n_h$ is the initial subgrade reaction modulus of sand, which can be obtained from API specification as a function of the sand friction angle; $\gamma$ is the soil weight density; $C_1$, $C_2$, and $C_3$ are non-dimensional coefficients that depend on the effective friction angle [6,7].

The approach commonly adopted in the literature describes the soil resistance to the lateral movement of a pile group through the use of a constant $p$-multiplier (i.e., the so-called group efficiency factor) equally applied to all piles of the group [2,5,8]. This group efficiency factor is commonly calculated as the average value of the $p$-multipliers for different pile rows and is adopted because different piles alternate the roles of leading and trailing piles during earthquake excitations. Figure 1 compares the $p$-multipliers for three-row pile groups obtained from the literature with the values recommended by the AASHTO specifications as a function of the ratio S/D [9]. The values suggested by AASHTO refer to pile groups with three or more rows in the load direction; they are equal to 0.8, 0.4, and 0.3 for the first, second, and third or higher row, respectively, when $S = 3D$, and to 1.0, 0.85, and 0.7, respectively, when $S = 5D$. A linear interpolation (shown in Figure 1) is used to determine the $p$-multiplier for pile spacing contained between $3D$ and $5D$. These values are found to be generally in good agreement with the $p$-multipliers obtained from the literature.

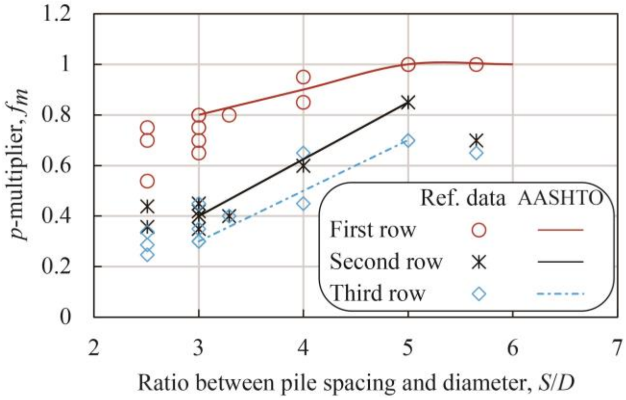


*Figure 1. p-multipliers for three-row pile groups in the sand (Data from* [10]*).*

However, the constant reduction factor cannot correctly simulate the difference of lateral soil resistance among different rows in a pile group under earthquake loading, leading to inaccurate estimates of differential curvatures for piles in different rows. This study adopts a new practical modeling method, which simulates the soil resistance in front of a pile at depth $h$ by using two parallel springs consisting of (1) a common nonlinear $p$-$y$ spring and (2) a nonlinear asymmetric spring, as illustrated in Figure 2. This modeling method was proposed by Zhou et al.[10] for the first time and adopted in this study to investigate the impact of different pile group effect modeling methods on the seismic behavior of pile group supported bridges. The $p$-$y$ spring is simulated using the uniaxial material *PySimple1* in OpenSees [11], and the corresponding input parameters are determined as given as follows:

$$p_{sym}^{(n)} = f_{m,t}^{(n)} \cdot p \tag{5}$$

$$p_{ult} = f_{m,t}^{(n)} \cdot p_u \cdot L_t \tag{6}$$

$$y_{50} = \frac{A \cdot p_u}{2n_h \cdot h} \cdot \ln\left(\frac{2A+1}{2A-1}\right) \tag{7}$$

where $p_{sym}^{(n)}$ denotes the soil resistance for the $n$-th row piles provided by the symmetric *p*-*y* spring. The superscript $n$ = 1, 2, …, $n_{\max}$ denotes the pile row number, and $n_{max}$ is the total number of rows. $p_{ult}$ denotes the ultimate soil resistance provided by the symmetric *p*-*y* spring; $y_{50}$ denotes the soil displacement at 50% of $p_{ult}$; $L_t$ denotes the tributary length of the soil-pile contact associated with the given node.

The nonlinear asymmetric spring is modeled using the uniaxial material *QzSimple1* in OpenSees [11], which has a behavior similar to the constitutive model for the *p*-*y* spring on the compression side but has an asymmetric and smaller soil strength on the tension side. The parameters of the backbone *q*-*z* curve are adjusted to approximately reproduce the same backbone curve used for the *p*-*y* spring, whereas the suction factor is set equal to zero. This nonlinear asymmetric spring is used to model the asymmetric value of the *p*-multiplier of any given pile when a pile group is subject to seismic loads, i.e., when two different *p*-multiplier values need to be applied to the same pile in a given row that is switching from leading (corresponding to the larger *p*-multiplier value, $f_{m,l}$ ) to trailing pile (corresponding to the smaller *p*-multiplier value, $f_{m,t}$ ) as the load changes direction. The asymmetric spring is oriented so that the compression side coincides with the side in which the pile is non-trailing. Thus, the soil resistances of the two parallel springs are given as follows:

$$p_{asym}^{(n)} = ( f_{m,l}^{(n)} - f_{m,t}^{(n)}) \cdot p \tag{8}$$

$$q_{ult} = ( f_{m,l}^{(n)} - f_{m,t}^{(n)}) \cdot p_u \cdot L_t \tag{9}$$

$$z_{50} = y_{50} \tag{10}$$

where $p_{asym}^{(n)}$ denotes the soil resistance for the $n$-th row piles provided by the asymmetric spring. The $q_{ult}$ denotes the ultimate soil resistance provided by the asymmetric *q*-*z* spring; $z_{50}$ denotes the soil displacement at 50% of $q_{ult}$, respectively. It is noted here that, for cases in which the *p*-multiplier value for a pile row remains constant in the two opposite loading directions, the soil resistance corresponding to this pile row can be modeled more simply by using only the symmetric *p*-*y* springs with the appropriate value of the *p*-multiplier. For example, when a pile group foundation in sandy soil has three rows of piles in the loading direction with a 3*D* pile spacing, the *p*-multiplier values are: $f_{m,l}^{(1)} = f_{m,l}^{(3)} = 0.8$, $f_{m,t}^{(1)} = f_{m,t}^{(3)} = 0.3$, and $f_m^{(2)} = f_{m,l}^{(2)} = f_{m,t}^{(2)} = 0.4$ .

## NUMERICAL MODEL DESCRIPTION

### Numerical model

A typical 2×3 pile group supported regular RC girder bridge in sandy soil with equal spans rested on single piers is selected as the prototype. The center-to-center space of the piles is 3*D*, and *D* is the pile diameter. The selected soil-bridge system is simplified as a 2×3 pile group supported single pier structure rather than using the FE model of the full bridge to reduce computational costs. In this simplified bridge model, the superstructure mass, calculated according to the axial load ratio of the pier (denoted as $\eta$), is lumped on the pier head. The earthquake shaking direction is applied along the 3-row pile direction since the 3-row piles can better reflect the pile group effect. This study analyzes two scenarios (i.e. the scour depth equal to 8 m and without scour scenario). The uncertainty of geotechnical and structural parameters is considered for each scenario. The considered parameters include thirteen structure-related parameters and one soil-related parameter, as listed in Table 1. A Latin hypercube sampling (LHS) technique is used to generate 80 soil-bridge system samples for each scenario based on the probability distribution of the fourteen parameters [12]. These samples are then randomly paired with 80 selected ground motion records, detailed in the next section.

*Table 1. Parameter uncertainty treatment.*

| Variable | Descripsion (unit) | Distribution | Mean | COV (%) | Lower | Upper | Ref. |
|---|---|---|---|---|---|---|---|
| $d$ | pile diameter (m) | Normal | 1.2 | 10 | 0.90 | 1.49 | [13] |
| $\rho_{l,p}$ | Longitudinal reinforcement ratio of pile | Normal | 0.01 | 27 | 0.0023 | 0.0170 | [14] |
| $\rho_{s,p}$ | Transverse reinforcement ratio of pile | Normal | 0.005 | 42 | 0.0003 | 0.0113 | [14] |
| $h_p$ | Pier height (m) | Normal | 6.5 | 26 | 2.27 | 11.32 | [14] |
| $d_c$ | Pier diameter (m) | Normal | 2 | 10 | 1.46 | 2.61 | [13] |
| $\rho_{l,c}$ | Longitudinal reinforcement ratio of pier | Normal | 0.015 | 27 | 0.0007 | 0.0284 | [14] |
| $\rho_{s,c}$ | Transverse rein. Ratio of pier | Normal | 0.005 | 42 | 0.0002 | 0.0105 | [14] |
| $f_c$ | Concrete strength (MPa) | Lognormal | 34.5 | 18 | 19.92 | 59.05 | [15] |
| $f_y$ | Reinforcement strength (MPa) | Lognormal | 420 | 10.6 | 319.23 | 549.14 | [16] |
| $E_s$ | Elastic modulus of rein. (MPa) | Lognormal | 201 | 3.3 | 184.28 | 219.60 | [16] |
| $\kappa$ | Hardening ratio of reinforcement | Lognormal | 0.0083 | 43 | 0.0026 | 0.0236 | [17] |
| $\eta$ | Axial load ratio | Normal | 0.1 | 12 | 0.0656 | 0.1336 | [13] |
| $G_b$ | Shear modulus of rubber (kPa) | Uniform | 900 | 22 | 500 | 1300 | [18] |
| $D_r$ | Sand relative density (%) | Uniform | 75 | 19 | 60 | 90 | [19] |

The finite element model of the studied soil-bridge system is generated in *OpenSees* based on the beam on a nonlinear Winkler foundation (BNWF) approach, as illustrated in Figure 2. The pile and pier are modeled using displacement-based beam-column elements with distributed plasticity [4,16,20]. The unconfined concrete of the pile and pier is represented by the uniaxial material *Concrete 01*, and the confined concrete of the pile and pier is modeled by the uniaxial material *Concrete 04.* The longitudinal steel reinforcements of the pile and pier are simulated by uniaxial material *Steel 02*, corresponding to the Menegotto-Pinto model with kinematic and isotropic strain hardening [21]. The element length of the pile and pier takes the value corresponding to their diameter, respectively. The pile cap is modeled by two elastic elements. The soil domain is represented by four-node Quad elements. Inspired by Aygün et al. [22], the soil domain sizes along and perpendicular to the shaking direction are equal to 40 m and 100 m, respectively. The size of the Quad element along the deep direction (i.e., Y-axis) takes 1$D$ ($D$ is the pile diameter) to match the pile element discretization. The *equalDOF* command is assigned to the nodes on opposite sides of the soil domain to simulate its pure-shear deformation[23]. Pressure-dependent multi-yield (PDMY) material is assigned to the Quad element to represent the constitutive model of the sandy soil, which corresponds to the Von Mises multi-surface kinematic plasticity model [24,25]. The model parameters of the sandy soil are determined according to literature-recommended methods, as listed in Table 2. A bilinear force-displacement constitutive model is used to simulate the elastomeric bearing. The constitutive model of the elastomeric bearing refers to Zhang and Huo [26]. The shear modulus of rubber (i.e., $G_b$) takes the sampling values through the LHS. The thickness of rubber (i.e., $t_b$) takes 0.07 m, and the total area of the bearing (i.e., $A_b$) is determined according to AASHTO by assuming the axial stress of rubber equals 11 MPa [9]. The 2D soil elements are linked to the 3D pile elements through soil springs to transfer the ground responses.

The lateral soil resistance is modeled considering the pile group effect. To investigate pile group effect modeling methods on the seismic behavior of pile group supported bridges, the above two pile group effect modeling methods are adopted and compared in this study. The vertical soil-pile friction behavior is simulated using *t-z* spring modeled with the *TzSimple1* material in OpenSees [11]. The corresponding input parameters $t_{ult}$ and $z_{50}$ are given by [27]:

$$t_{ult} = k_0 \cdot \gamma \cdot h \cdot \pi \cdot D \cdot L_t \cdot \tan(0.8\phi \cdot \pi / 180) \tag{11}$$

$$z_{50} = \frac{t_{ult}}{k \cdot \pi \cdot D \cdot L_t} \tag{12}$$

where $t_{ult}$ is the ultimate friction force at the soil-pile interface within the tributary length $L_t$. $k_0$ is the coefficient of lateral earth pressure at rest and is set equal to 0.4. $\phi$ is the friction angle of sand; $z_{50}$ is the displacement at which the friction force reaches 50% of $t_{ult}$; $k$ denotes the initial tangent stiffness and can be expressed as a function of the friction angle [27].

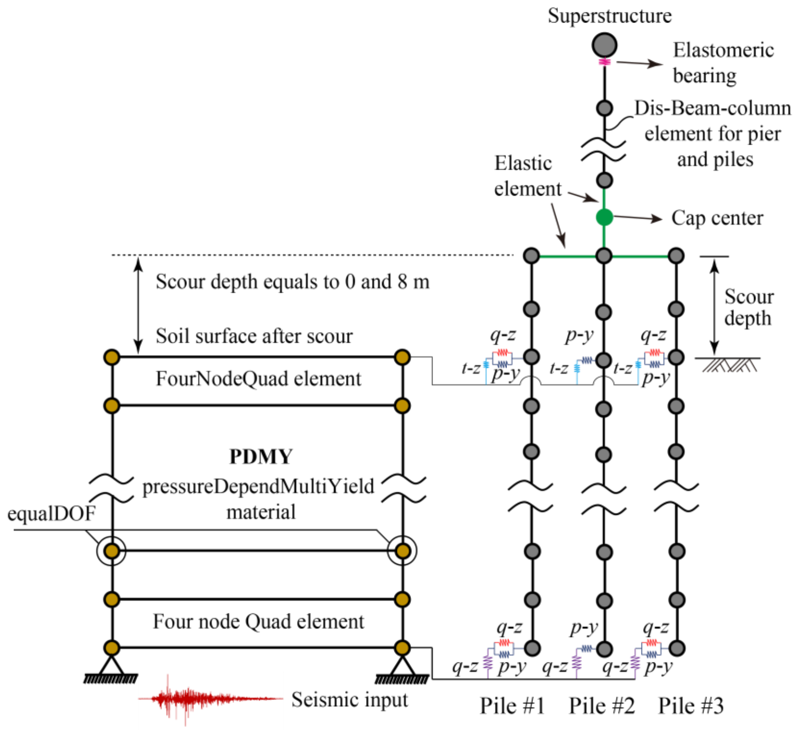


*Figure 2. FE model of the studied soil-bridge system.*

*Table 2. Parameters for the constitutive models (PDMY) of sandy soil.*

| Parameter (unit) | Description and source |
|---|---|
| *$Dr$ (%) | Relative density of the test sand, taking the sampling value. |
| *$G_s$ (ton/m$^3$) | Empirical specific density, taking 2.65 [28]. |
| * $e_{min}$ | The minimum initial void ratio of sand, taking 0.894 [13]. |
| * $e_{max}$ | The maximum initial void ratio of sand, taking 0.516 [13]. |
| $e$ | Initial void ratio $e = e_{max} - D_r(e_{max} - e_{min})$ [28] |
| *$Vs$ (m/s) | Shear wave velocity $V_s = 85(N_{1,60} + 2.5)^{0.25}$, $N_{1,60} = 60D_r^2$ [13,29]. |
| $\rho_{sat}$ (ton/m3) | Saturated density, $\rho_{sat} = \rho_w(G_s + e)/(1+e)$ [28]. |
| *$G_{\max}$ (kPa) | Maximum shear modulus, $G_{max} = \rho V_s^2$ [29–31]. |
| $G_r$ (kPa) | Reference low-strain shear modulus, $G_r = \sqrt{1.5}G_{max}$ [29]. |
| * $\nu$ | Poison's ratio, taking 0.33 [13,29] |
| $B_r$ (kPa) | Reference bulk modulus, $B_r = 2G_r(1+\nu)/(3-6\nu)$ [25,29] |
| $\phi$ (degree) | Friction angle, $\varphi = 16D_r^2 + 0.17D_r + 28.4$ [32]. |
| $c$ | The rate of shear-induced volume decrease, $c = -0.024\ln(100D_r) + 0.124$ [13]. |
| $\gamma_{\max}$ | An octahedral shear strain at failure at the reference mean effective pressure $p_r$, taking 0.1. |
| $p_r$ (kPa) | Reference mean effective confining pressure at which $G_r$, $B_r$, and $\gamma_{\max}$ are defined, taking 80. |
| $c_p$ | Pressure dependence coefficient, taking 0.5. |
| $\phi_{PT}$ (degree) | Phase transformation angle, taking 27. |
| $Dil_1$<br>$Dil_2$ | $Dil_1$ and $Dil_2$ denote the non-negative constants defining the rate of shear-induced volume increase (dilation), taking 0.4 and 2, respectively. |

### Ground motions

To consider the uncertainty of ground motions, a set of 80 unscaled ground motions from rock sites is selected from the PEER NGA-West2 Database [33]. Figure 3a shows the 5%-damped acceleration spectra of the selected 80 ground motions. The first-order vibration period of the studied soil-bridge system in the shaking direction varies between 0.89 and 2.13 seconds and is colored in Figure 3.

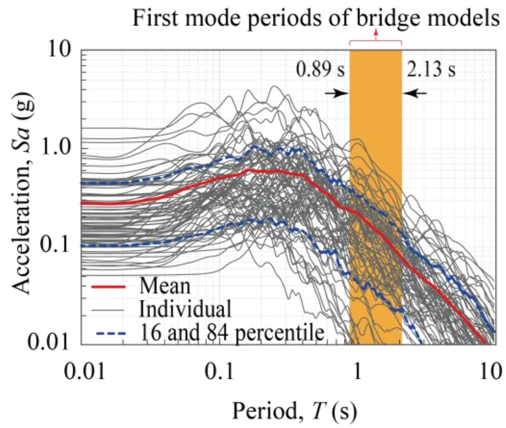


*Figure 3. 5%-damped acceleration response spectra.*

### Sensitivity analysis for the soil element discretization

In order to capture a stable seismic response of the soil-bridge system, sensitivity analyses for the soil element discretization are carried out in this study. Eight soil element discretization schemes are compared in this study, as shown in Figure 4. It is found that the soil element number and size along the shaking direction have an extremely slight influence on the soil-bridge system response when the size of the soil column along the shaking direction is larger than 10 m. In addition, almost identical responses are recorded when the thickness of the soil domain equals 20 m and 100 m.

## THE INFLUENCE ANALYSES OF DIFFERENT PILE GROUP EFFECT MODELING METHODS

Figure 5 presents the impact of different pile group modeling methods on the embedded depth of the belowground pile shaft. Two different scour scenarios (i.e., the scour depth equal to 0 and 8 m) are investigated. As shown in the figure, the existing pile group effect modeling method (i.e., the pile group efficiency method) could overestimate the embedded depth of the plastic hinge of the leading pile and underestimate the plastic hinge embedded depth of trailing piles. It is also found that the average embedded depth of the belowground plastic hinge of the leading pile shaft is less than that of the trailing pile when adopted the proposed pile group effect modeling method. This result is identical to the quasi-static test finding reported by Zhou et al. [1]. However, the opposite trend is recorded using the existing pile group effect modeling method.

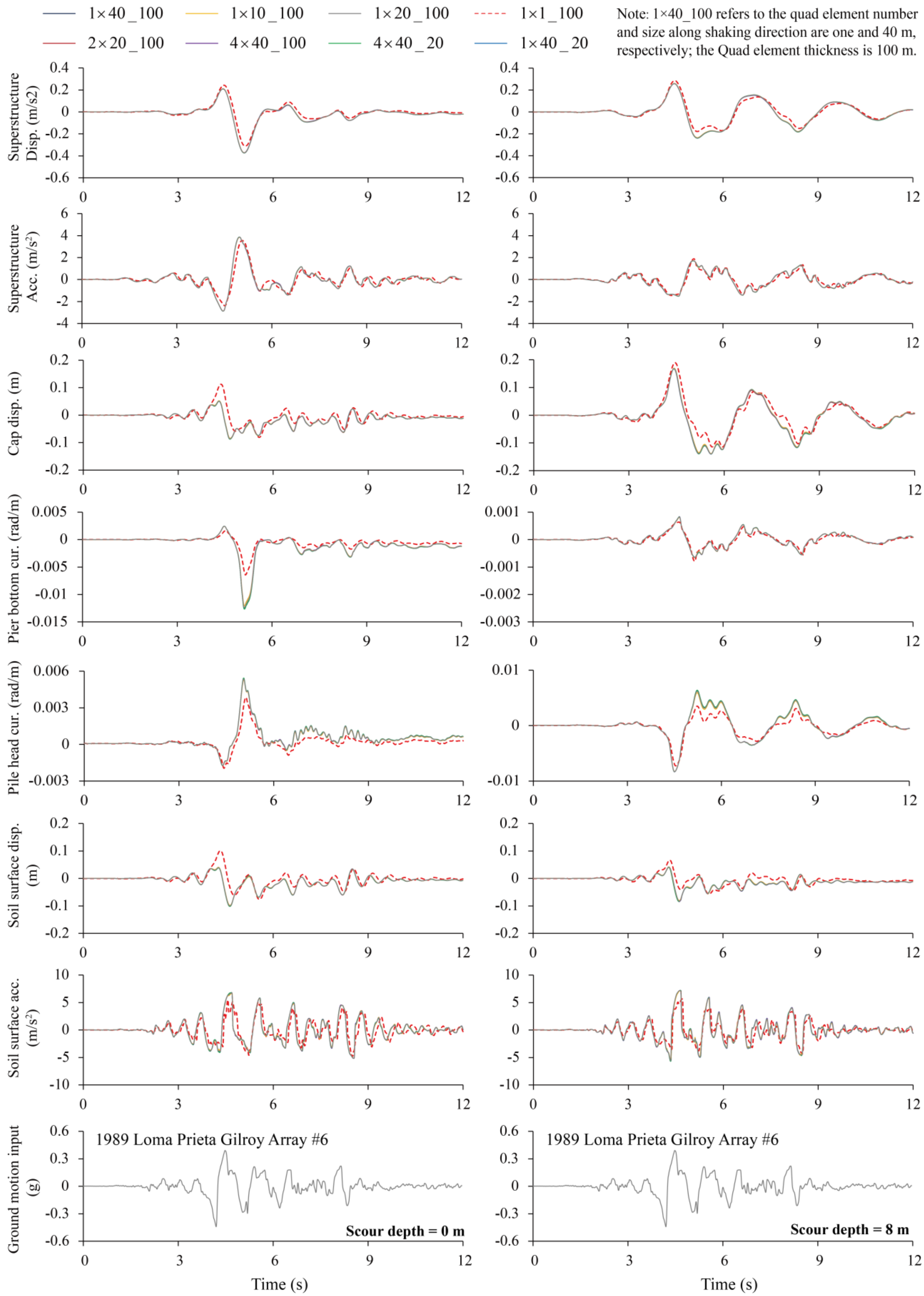


*Figure 4. Sensitivity analyses for the soil element discretization.*

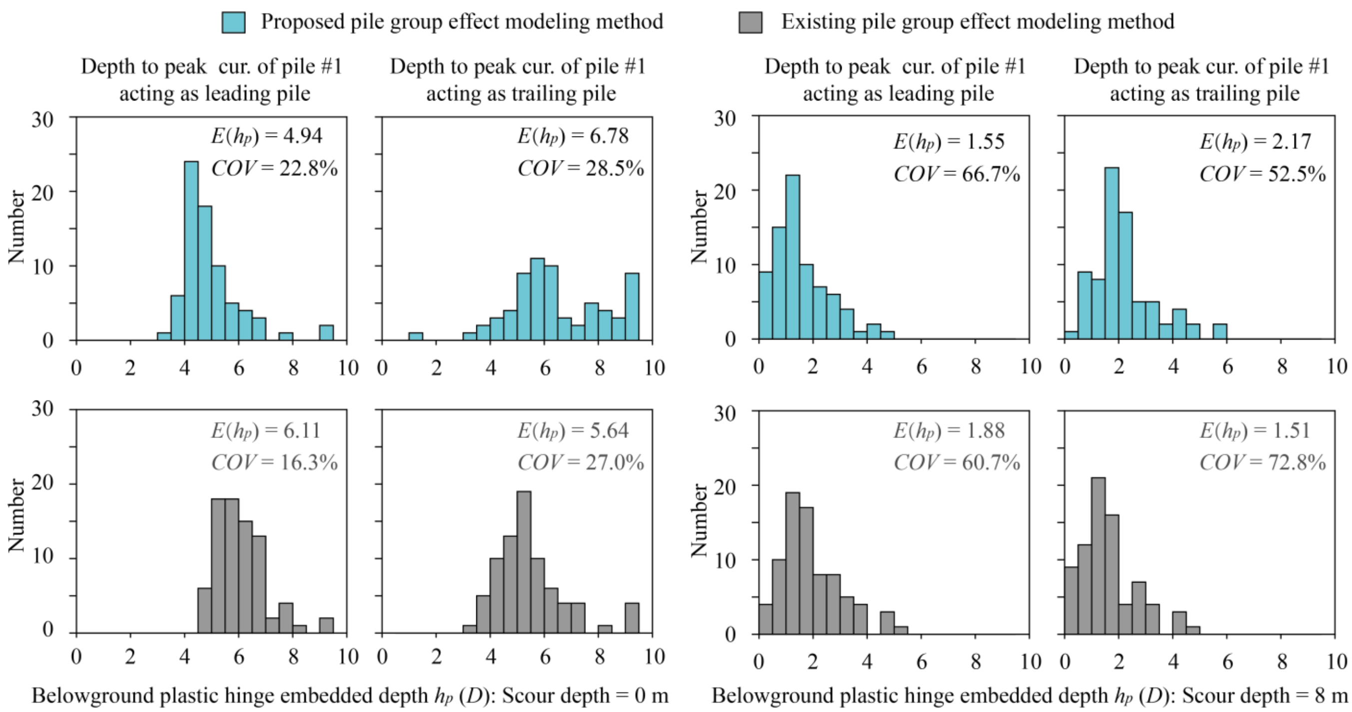


*Figure 5. The influence of the pile group effect modeling method on the belowground plastic hinge embedded depth.*

Table 3 lists the average relative error (defined by Eq. 13) for different engineering demand parameters of the pile-bridge system predicted through the different pile group effect modeling methods, including the peak curvature demand of pile head and pile shaft, the peak curvature demand of pier bottom section, and the peak displacement demand of bearing. As listed in Table 3, compared with the pile group modeling method proposed in this study, the existing pile group efficiency method could significantly underestimate the curvature demand of the pile head and shaft. It is found that the pile group effect modeling methods have a slight effect on the pier curvature demand and bearing displacement demand.

$$\varepsilon = \frac{1}{N}\sum_{i=1}^{N}\psi_i \tag{13}$$

$$\psi_i = \frac{D_{\mathrm{P},i} - D_{E,i}}{D_{\mathrm{P},i}} \tag{14}$$

where $\psi_i$ is the relative error for the *i*-th case, and *N* is the total number of the analyzed cases and equals 80 in this study. $D_{\mathrm{P},i}$ denotes the *i*-th demand predicted using the proposed pile group effect modeling method in this study. $D_{E,i}$ denotes the *i*-th demand predicted using the existing pile group effect modeling method.

*Table 3. The average relative error for different EDP values.*

| Engineering demand parameters | S0 | S8 |
|---|---|---|
| Peak curvature of pile head | **20.90%** | **12.60%** |
| Peak curvature of belowground pile shaft | **19.16%** | **8.62%** |
| Peak curvature of pier bottom section | -0.07 % | -0.52% |
| Peak displacement of bearing | -0.03% | -0.44% |

The Fragility curve presents the conditional failure probability of a selected component at the given ground motion intensity, which considers the uncertainty of demand and capacity of the selected component. The fragility curve is generated through Eqs 15 to 17.

$$P[D \geq LS_i \mid IM] = 1 - \Phi\left(\frac{\ln(S_C) - \ln(S_D)}{\sqrt{\beta_{D|IM}^2 + \beta_C^2}}\right) \tag{15}$$

$$\ln(S_D) = \ln(a) + b\ln(IM) \tag{16}$$

$$\beta_{D|IM} = \sqrt{\frac{\sum_{i=1}^{N}(\ln(D_i) - \ln(S_D))^2}{N-2}} \tag{17}$$

Where $LS_i$ is the limit state threshold. $S_c$ is the mean value of the capacity, and $S_D$ is the mean value estimation of the seismic demand. $\beta_{D|IM}$ is dispersion estimation of the seismic demand. $a$ and $b$ is the regression coefficient for the probabilistic seismic demand model. $D_i$ is the $i$-th estimation value of the seismic demand, and $N$ is the total number of the seismic demand for the considered component.

The velocity spectrum intensity (VSI) is selected as the IM to generate the seismic fragility curves [34]. As shown in Figure 6, the existing group efficiency method could underestimate the seismic fragility of the pile head. However, it slightly affects the seismic fragility of pile shafts, pier, and rubber bearings. In addition, the scour increases the seismic fragility of the pile foundation. Still, it could have a slight impact on the seismic fragility of the pier and bearings for the pile-group supported bridges, as presented in Figure 7.

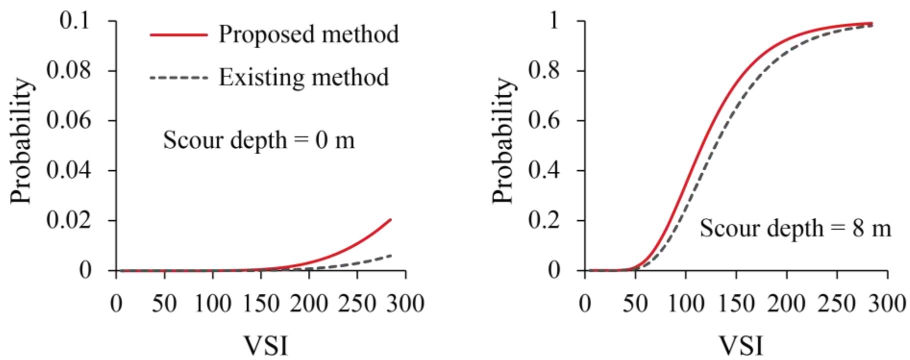


(a) Slight damage fragility curve for pile head

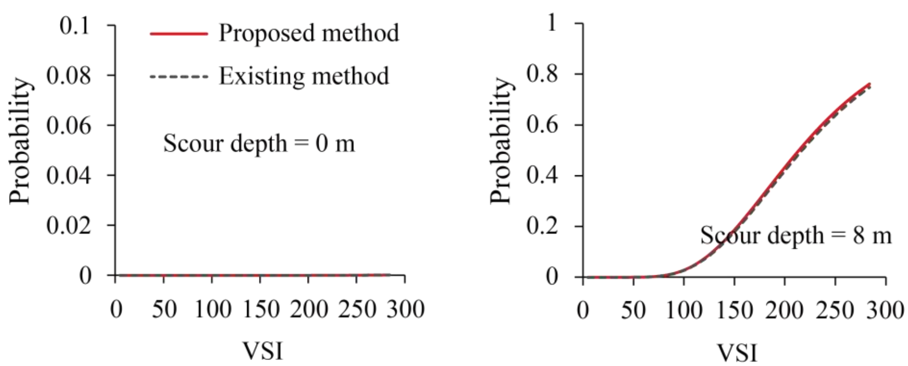


(b) Slight damage fragility curve for belowground pile shaft

*Figure 6. Influence of pile group effect modeling methods on the seismic fragility of piles.*

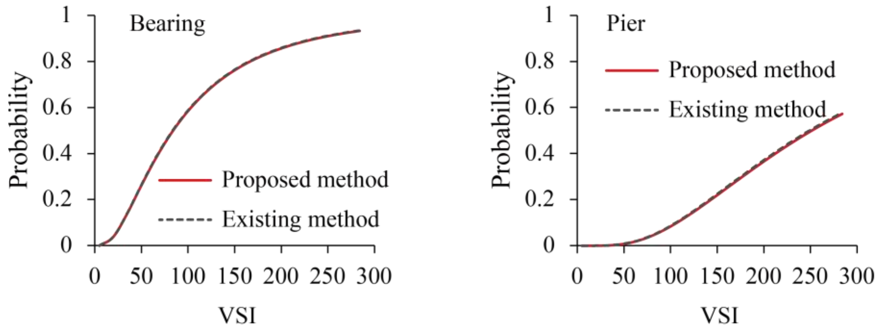


*Figure 7. Influence of pile group effect modeling methods on the seismic fragility of bearing and pier (Scour depth = 8 m).*

## CONCLUSIONS

The main conclusions of this study are summarized as follows:

(1) The pile group effect modeling method proposed in this study can better predict the nonlinear seismic behavior of pile group-supported bridges.

(2) The commonly used pile group efficiency method could underestimate the seismic demand or fragility of the pile head.

(3) The pile group effect modeling methods slightly affect the global seismic response of the pile group supported bridges, including the pier curvature and bearing displacement demand.

## ACKNOWLEDGMENTS

The authors gratefully acknowledge the funding support of this work by the National Natural Science Foundation of China (Grant No. 51778469 and 52178155). Special thanks to Professor Michele Barbato and Professor Ross W. Boulanger at the University of California, Davis, who provided significant suggestions on the modeling of the pile group effect under cyclic loading. Any opinions, findings, and conclusions expressed are those of the authors and do not necessarily reflect those of the sponsoring organizations.

## REFERENCES

[1] Zhou L, Barbato M, Ye A. Experimental investigation of postearthquake vertical load-carrying capacity of scoured reinforced concrete pile group bridge foundations. J Bridg Eng 2021;26:1–14. https://doi.org/10.1061/(ASCE)BE.1943-5592.0001799.

[2] Liu T, Wang X, Ye A. Roles of pile group and cap-rotation effects on seismic failure mechanisms of partially-embedded bridge foundations: Quasi-static tests. Soil Dyn Earthq Eng 2020;132:106074. https://doi.org/10.1016/j.soildyn.2020.106074.

[3] Wang X, Ye A, He Z, Shang Y. Quasi-static cyclic testing of elevated rc pile-cap foundation for bridge structures. J Bridg Eng 2016;21:04015042. https://doi.org/10.1061/(ASCE)BE.1943-5592.0000797.

[4] Wang Z, Dueñas-Osorio L, Padgett JE. Influence of scour effects on the seismic response of reinforced concrete bridges. Eng Struct 2014;76:202–14. https://doi.org/10.1016/j.engstruct.2014.06.026.

[5] Lemnitzer A, Khalili-Tehrani P, Ahlberg ER, Rha C, Taciroglu E, Wallace JW, et al. Nonlinear efficiency of bored pile group under lateral loading. J Geotech Geoenvironmental Eng 2010;136:1673–85. https://doi.org/10.1061/(ASCE)GT.1943-5606.0000383.

[6] API (American Petroleum Institute). Recommended practice for planning, designing and constructing fixed offshore platforms - working stress design. 2007.

[7] Chai YH, Song S-T. Inelastic deformation of extended pile-shafts. J Eng Mech 2012;138:842–52. https://doi.org/10.1061/(ASCE)EM.1943-7889.0000393.

[8] Adeel MB, Jan MA, Aaqib M, Park D. Development of simulation based p-multipliers for laterally loaded pile groups in granular soil using 3d nonlinear finite element model. Appl Sci 2020;11:26. https://doi.org/10.3390/app11010026.

[9] AASHTO (American Association of State Highway and Transportation Officials). AASHTO LRFD bridge design specifications. Washington, D.C.: 2020.

[10] Zhou L, Barbato M, Ye A. Pile group effect modelling and parametric sensitivity analysis of scoured pile group bridge foundations in sandy soils under lateral loads. J Bridg Eng 2023;28. https://doi.org/10.1061/JBENF2.BEENG-5861.

[11] Boulanger RW, Curras CJ, Kutter BL, Wilson DW, Abghari A. Seismic soil-pile-structure interaction experiments and analyses. J Geotech Geoenvironmental Eng 1999;125:750–9. https://doi.org/10.1061/(ASCE)1090-0241(1999)125:9(750).

[12] Olsson A, Sandberg G, Dahlblom O. On Latin hypercube sampling for structural reliability analysis. Struct Saf 2003;25:47–68. https://doi.org/10.1016/S0167-4730(02)00039-5.

[13] Wang X, Ye A, Ji B. Fragility-based sensitivity analysis on the seismic performance of pile-group-supported bridges in liquefiable ground undergoing scour potentials. Eng Struct 2019;198:109427. https://doi.org/10.1016/j.engstruct.2019.109427.

[14] Brandenberg SJ, Kashighandi P, Zhang J, Huo Y, Zhao M. Fragility functions for bridges in liquefaction-induced lateral spreads. Earthq Spectra 2011;27:683–717. https://doi.org/10.1193/1.3610248.

[15] Pang Y, Wu X, Shen G, Yuan W. Seismic fragility analysis of cable-stayed bridges considering different sources of uncertainties. J Bridg Eng 2014;19:1–11. https://doi.org/10.1061/(ASCE)BE.1943-5592.0000565.

[16] Barbato M, Gu Q, Conte JP. Probabilistic push-over analysis of structural and soil-structure systems. J Struct Eng 2010;136:1330–41. https://doi.org/10.1061/(ASCE)ST.1943-541X.0000231.

[17] Zhou L, Shahria Alam M, Song A, Ye A. Probability-based residual displacement estimation of unbonded laminated rubber bearing supported highway bridges retrofitted with Transverse Steel Damper. Eng Struct 2022;272:115053. https://doi.org/10.1016/j.engstruct.2022.115053.

[18] Stefanidou SP, Kappos AJ. Methodology for the development of bridge-specific fragility curves. Earthq Eng Struct Dyn 2017;46. https://doi.org/10.1002/eqe.2774.

[19] Jones AL, Kramer SL, Arduino P. Estimation of Uncertainty in Geotechnical Properties for Performance-Based Earthquake Engineering Estimation of Uncertainty in Geotechnical Properties for Performanced-Based Earthquake Engineering 2002.

[20] Zhou L, Ye A, Chen F. Postearthquake vertical load-carrying capacity of extended pile shafts in cohesionless soils: quasi-static test and parametric studies. J Bridg Eng 2022;27:1–16. https://doi.org/10.1061/(asce)be.1943-5592.0001918.

[21] Filippou FC, Popov EP, Bertero VV. Effects of bond deterioration on hysteretic behaviour of reinforced concrete joints. 1983.

[22] Aygün B, Dueñas-Osorio L, Padgett JE, DesRoches R. Efficient longitudinal seismic fragility assessment of a multispan continuous steel bridge on liquefiable soils. J Bridg Eng 2011;16:93–107. https://doi.org/10.1061/(ASCE)BE.1943-5592.0000131.

[23] Wang X, Shafieezadeh A, Ye A. Optimal intensity measures for probabilistic seismic demand modeling of extended pile-shaft-supported bridges in liquefied and laterally spreading ground. Bull Earthq Eng 2018;16:229–57. https://doi.org/10.1007/s10518-017-0199-2.

[24] Elgamal A, Yan L, Yang Z, Conte JP. Three-dimensional seismic response of Humboldt Bay bridge-foundation-ground system. J Struct Eng 2008;134:1165–76. https://doi.org/10.1061/(ASCE)0733-9445(2008)134:7(1165).

[25] Yang Z, Elgamal A, Parra E. Computational model for cyclic mobility and associated shear deformation. J Geotech Geoenvironmental Eng 2003;129:1119–27. https://doi.org/10.1061/(ASCE)1090-0241(2003)129:12(1119).

[26] Zhang J, Huo Y. Evaluating effectiveness and optimum design of isolation devices for highway bridges using the fragility function method. Eng Struct 2009. https://doi.org/10.1016/j.engstruct.2009.02.017.

[27] Mosher RL. Load-transfer criteria for numerical analysis of axially loaded piles in sand. Part 1 Load-transfer criteria. U. S. Army Engineer Waterways Experiment Station. Vicksburg, Miss: 1984.

[28] Das BM. Principles of foundation engineering. Seventh ed. Stamford, USA: Cengage Learning; 2011.

[29] Khosravifar A, Elgamal A, Lu J, Li J. A 3D model for earthquake-induced liquefaction triggering and post-liquefaction response. Soil Dyn Earthq Eng 2018;110:43–52. https://doi.org/10.1016/j.soildyn.2018.04.008.

[30] Rollins KM, Evans MD, Diehl NB, III WDD. Shear modulus and damping relationships for gravels. J Geotech Geoenvironmental Eng 1998;124:396–405. https://doi.org/10.1061/(ASCE)1090-0241(1998)124:5(396).

[31] Lysmer J, Kuhlemeyer RL. Finite dynamic model for infinite media. J Eng Mech Div 1969;95:859–77. https://doi.org/10.1061/JMCEA3.0001144.

[32] Rollins KM, Lane JD, Gerber TM. Measured and computed lateral response of a pile group in sand. J Geotech Geoenvironmental Eng 2005;131:103–14. https://doi.org/10.1061/(ASCE)1090-0241(2005)131:1(103).

[33] Ancheta TD, Darragh RB, Stewart JP, Seyhan E, Silva WJ, Chiou BSJ, et al. NGA-West2 Database. Earthq Spectra 2014;30:989–1005. https://doi.org/10.1193/070913EQS197M.

[34] Zhou L, Alam MS, Wang X, Ye A, Zhang P. Optimal intensity measure selection and probabilistic seismic demand model of pile group supported bridges in sandy soil considering variable scour effects. Ocean Eng 2023;285:115365. https://doi.org/10.1016/j.oceaneng.2023.115365.